ELSEVIER

Surface Science 326 (1995) 335–346

surface science

Determination of electron lifetime at low energies from sp-band photoemission

A. Beckmann

Max-Planck-Institut für Mikrostrukturphysik, Weinberg 2, D-06120 Halle, Germany

Received 31 October 1994; accepted for publication 30 November 1994

Abstract

The photoelectric current is calculated on the basis of the Green's function matching method. Peak widths and intensities of bulk and surface states are studied in dependence on electron and hole lifetimes. For Cu(111) it is shown that the ratio of peak intensities of both types of states yield information on electron inverse lifetime which can particularly be used for very low energies (< 10 eV), where the peak width analysis for studying lifetimes fails.

Keywords: Angle resolved photoemission; Copper; Electron density, excitation spectra calculations; Green's function methods; Photoelectron emission; Semi-empirical models and model calculations; Surface electronic phenomena

1. Introduction

The direct method of investigating electron and hole lifetimes in valence-band photoemission ($\omega < 20$ eV) consists in determining the full width at half maximum (FWHM) in angular-resolved spectra [1–8]. Provided that broadening contributions from the analyzing process are known, it is still necessary to eliminate contributions to the FWHM from initial and final state bands. In general, this is done by using a special spectroscopic tuning mode (e.g. constant initial state spectroscopy) but the technique is restricted to certain suitable energies (e.g. the initial state energy is near the Fermi level). For very low electron energies (< 10 eV) in particular there are almost no electron lifetimes available from photoemission.

To our knowledge the relation between lifetimes and peak intensities has not yet been investigated. Obviously, the correspondence is somewhat problematic since intensities additionally depend on optical absorption and electron scattering. In the simplest way of a one-step formulation of photoemission, scattering only appears in the self-energies of the photohole and photoelectron. It results in a mean free path or a complex $k_\perp$, respectively, by means of band dispersion. Vertex corrections are neglected. Inelastic scattering is assumed to depend weakly on energy on the scale of interest. To be independent of these corrections, only the ratio of the bulk peak intensity to the surface state peak intensity is considered.

It is at least necessary to show that bulk and surface state peaks differ in their dependences on lifetimes. Especially the surface state peak characteristics are not yet satisfactorily understood. On the one hand, there are computer programs which are based on the dynamic scattering formulation of photoemission [9]. In this way one can calculate the FWHM with electron and hole lifetimes being the input parameters [10]. On the other hand, a

SSDI 0039-6028(94)00798-5

simple golden-rule formula for the emission from bulk states, including a Lorentzian broadening, yields the following FWHM of the energy distribution curve (EDC) [8]:

$$\tilde{\gamma}_b = \left(\frac{\gamma_1}{|v_1|} + \frac{\gamma_2}{|v_2|} \right) \left| \frac{1}{|v_1|} \left(1 - \frac{v_{1\parallel} \sin^2(\theta)}{k_\parallel} \right) - \frac{1}{|v_2|} \left(1 - \frac{v_{2\parallel} \sin^2(\theta)}{k_\parallel} \right) \right|^{-1}, \tag{1}$$

where γ_1 and γ_2 are given by the imaginary parts of the optical potential for the hole and the electron, respectively, i.e., $\gamma_E = -2 \operatorname{Im} \Sigma(E)$. $E = E_1$ and $E = E_2 = E_1 + \omega$ are the initial and final state energies, v_1 and v_2 are the corresponding velocities perpendicular to the surface, $v_{1\parallel}$ and $v_{2\parallel}$ are the corresponding parallel velocities, and θ is the angle with respect to the surface normal. For $\theta = 0$, formula (1) is usually quoted in the literature [1–6]. Now one might argue that for the surface state $\tilde{\gamma}_s$ should be obtained from (1) with $v_1 = 0$ since there is no perpendicular dispersion. Queerly, the result turns out to be correct in spite of the argument being wrong. The derivation of Eq. (1) is based on the "quasi-$k_\perp$-conservation" [8] which is commonly derived for bulk state transitions where complex $k_\perp$ is simply a consequence of the absorbing potential. This corresponds to a Lorentzian broadening of the spectral functions which belong to the internal current passing a plane from one side. The situation for a matched system is completely different. Though being possibly stable, the surface state has a complex $k_\perp$, which results from a complex band structure within a hybridizing gap. Matching requires the superposition of propagating and evanescent waves, not only for surface states but for bulk states, too. Hence, the correct way is to derive $\tilde{\gamma}_b$ and $\tilde{\gamma}_s$ from the corresponding poles of the current, which actually are different as it will be shown below by using complex band structure and matching. In addition, some other facts can also be deduced only by applying a correct analysis, for example the broadening of surface and bulk peaks resulting from different kinds of defects [5–7], or the resonance of the surface state as a function of ω [11–14].

In order to include excitations from surface states, a "one-step model" of photoemission is required with the Green's functions determined for a matched or truncated system. This was carried out for a simple tight-binding model for initial states [15]. Although the model is not properly satisfying for calculating sp-bands, it enables surface and bulk peak characteristics to be calculated on the same basis.

In the present paper, the photoelectron current is rigorously calculated on the basis of a pseudopotential model using the method of Green's function matching [16,17]. The method was used by Paasch [18] mainly to determine the asymptotic expansion for the final state. Approximations are restricted to the free-electron based Hamiltonian, whereas integrations for determining the current are exactly performed. Although it is appropriate to use a free-electron basis for matching, the method is practically restricted to sp-bands. It is well known that photoemission matrix elements are not correctly obtained from a pseudopotential model, especially for initial states arising from well localized electrons. Besides revealing differences in bulk band emission and surface band emission in principle, the examination of the poles directly yields the corresponding intensities. For illustration, in Section 3 a simple nearly-free-electron two-band model is used to study photoemission in normal direction of Cu(111).

2. The photoelectric current

2.1. Formalism

Let the crystal fill the half space $x < 0$ with Q being the projection onto that space. The potential for $x > 0$ is continued by the surface barrier which asymptotically approaches the flat vacuum potential and which is assumed to be free of lateral corrugation. The current with the momentum component parallel to the surface $\boldsymbol{K}_\parallel$ and energy E is given by

$$I_X(\boldsymbol{K}_\parallel E) = -\frac{p_x}{\pi} \operatorname{Im} \left(X, \boldsymbol{K}_\parallel | \boldsymbol{G}_2^+ \Delta Q \boldsymbol{G}_1^+ Q \Delta^+ \boldsymbol{G}_2^- | X, \boldsymbol{K}_\parallel \right) + \text{surface barrier contributions}, \tag{2}$$

where X is the distance of the plane of detector from the surface. The neglected surface barrier contributions correspond to a similar expression with Q replaced by its complement $P = 1 - Q$. $G^{+}_{1,2}$ are the retarded hole and electron Green's functions and Δ is the coupling to the photon field,

$$\Delta = \tfrac{1}{2i}(\nabla \cdot A + A \cdot \nabla), \tag{3}$$

$$A = \sum_{\alpha} A_{\alpha} e^{i\kappa_{\alpha} x} e^{i\kappa_{\|} \rho}. \tag{4}$$

$A_{\alpha} = (A_{x\alpha}, A_{\|\alpha})$ are the longitudinal ($\alpha = \mathrm{L}$) and transversal ($\alpha = T$) components of the field. $\kappa_{\|}$ is real and $\mathrm{Im}(\kappa_{\alpha}) < 0$. The Green's functions are determined by their surface-projected parts $\mathscr{G}_{1,2}$ and the crystal and vacuum barrier functions $\mathscr{G}_{\mathrm{c}}$ and $\mathscr{G}_{\mathrm{b}}$ (and their surface-projected parts $\mathscr{G}_{\mathrm{c}}$ and $\mathscr{G}_{\mathrm{b}}$) [16,17]

$$\hat{G}(x,x') = \hat{G}_{\mathrm{c}}(x,x') + \hat{G}_{\mathrm{c}}(x,0)\hat{\mathscr{G}}_{\mathrm{c}}^{-1}\left(\hat{\mathscr{G}} - \hat{\mathscr{G}}_{\mathrm{c}}\right)\hat{\mathscr{G}}_{\mathrm{c}}^{-1}\hat{G}_{\mathrm{c}}(0,x'), \quad x,x' < 0, \tag{5}$$

$$\hat{G}(x,x') = \hat{G}_{\mathrm{b}}(x,0)\hat{\mathscr{G}}_{\mathrm{b}}^{-1}\hat{\mathscr{G}}\hat{\mathscr{G}}_{\mathrm{c}}^{-1}\hat{G}_{\mathrm{c}}(0,x'), \quad x > 0,\ x' < 0, \tag{6}$$

where E, $\boldsymbol{K}_{\|}$ are suppressed. Furthermore, the G's are matrices with respect to the parallel component of the reciprocal lattice vector $\boldsymbol{g}_{\|}$, i.e., $\boldsymbol{g} = (g, \boldsymbol{g}_{\|})$:

$$\left(\boldsymbol{g}_{\|}|\hat{G}_{\mathrm{c}}(x,x')|\boldsymbol{g}'_{\|}\right) \equiv G_{\mathrm{c}}(x,x',\boldsymbol{K}_{\|}+\boldsymbol{g}_{\|},\boldsymbol{K}_{\|}+\boldsymbol{g}'_{\|})$$

$$= \sum_{g,g'} \int \frac{dK}{2\pi} \exp[i(K+g)x - i(K+g')x']\, G_{\mathrm{c}}(\boldsymbol{K}+\boldsymbol{g},\boldsymbol{K}+\boldsymbol{g}'). \tag{7}$$

G_{b} at the energy $\epsilon = E - \mu k_{\|}^2$ is most simply represented by the wavefunctions in one dimension, which, for example, can be calculated by numerical integration of the Schrödinger equation with a certain barrier potential:

$$\mu_{\mathrm{b}} G_{\mathrm{b}}(x,x',\boldsymbol{K}_{\|}) = \frac{\psi_1(x,\boldsymbol{K}_{\|})\psi_2(x',\boldsymbol{K}_{\|})\theta(x-x') + \psi_2(x,\boldsymbol{K}_{\|})\psi_1(x',\boldsymbol{K}_{\|})\theta(x'-x)}{W(\psi_1,\psi_2)}. \tag{8}$$

μ_{b} is half the reciprocal free-electron mass, i.e., $\mu_{\mathrm{b}} = 1/2$ in atomic units. Asymptotically, ψ_1 and ψ_2 are ingoing and outgoing plane waves, and W is the Wronskian.

The matching Eq. [16,17] determines $\mathscr{G}$,

$$\hat{\mathscr{G}}^{-1} = \mu_{\mathrm{b}}{}'\hat{\mathscr{G}}_{\mathrm{b}}^{-}\hat{\mathscr{G}}_{\mathrm{b}}^{-1} - \mu_{\mathrm{c}}{}'\hat{\mathscr{G}}_{\mathrm{c}}^{+}\hat{\mathscr{G}}_{\mathrm{c}}^{-1} = \mu_{\mathrm{b}}\hat{\mathscr{L}}_{\mathrm{b}} - \mu_{\mathrm{c}}\hat{\mathscr{L}}_{\mathrm{c}}, \tag{9}$$

where from (5)

$${}'\mathscr{G}_{\mathrm{c}}^{+}(\boldsymbol{K}_{\|}+\boldsymbol{g}_{\|},\boldsymbol{K}_{\|}+\boldsymbol{g}'_{\|}) = \lim_{\eta\to 0^{+}} \sum_{g,g'} \int \frac{dK}{2\pi} e^{-iK\eta}(K+g)G_{\mathrm{c}}(\boldsymbol{K}+\boldsymbol{g},\boldsymbol{K}+\boldsymbol{g}'). \tag{10}$$

$\mu_{\mathscr{L}}$ is half the inverse effective mass of the crystal, which unlike to μ_{b} may deviate from the value $1/2$. $\mathscr{G}_{\mathrm{b}}$ and ${}'\mathscr{G}_{\mathrm{b}}^{-}$ are calculated by using (8) where the derivative has to be taken from the right unlike to (10). It is advantageous to represent the propagation of the electron through the surface in terms of transmission of the vacuum incoming wave. Using (6) and the vacuum Green's function G_0 yields the propagation from $x = X$ through the surface

$$\left(X,\boldsymbol{K}_{\|}|\boldsymbol{G}_2^{+} = \frac{e^{ip_x X}}{ip_x}\left(\boldsymbol{K}_{\|}|\mathscr{T}_2^{+}\boldsymbol{G}_{\mathrm{c}2}^{+\,-1}\mathscr{G}_{\mathrm{c}2}^{+}, \right.\right. \tag{11}$$

where the transmission amplitude is given by

$$(\boldsymbol{K}_{\|}|\mathscr{T}_2^{+}|\boldsymbol{K}_{\|}+\boldsymbol{g}_{\|}) = (X,\boldsymbol{K}_{\|}|G_2^{+}|0,\boldsymbol{K}_{\|}+\boldsymbol{g}_{\|})/(X,\boldsymbol{K}_{\|}|G_0^{+}|0,\boldsymbol{K}_{\|}) = \mathscr{T}_{20}(\boldsymbol{K}_{\|})\mathscr{G}_{\mathrm{b}}^{+\,-1}(\boldsymbol{K}_{\|})\mathscr{G}_2^{+}(\boldsymbol{K}_{\|},\boldsymbol{K}_{\|}+\boldsymbol{g}_{\|}), \tag{12}$$

$$\mathscr{T}_{20}(\boldsymbol{K}_{\|}) = (X,\boldsymbol{K}_{\|}|G_{\mathrm{b}}^{+}|0,\boldsymbol{K}_{\|})/(X,\boldsymbol{K}_{\|}|G_0^{+}|0,\boldsymbol{K}_{\|}), \tag{13}$$

X is far outside the surface where the expressions on the right of (12) and (13) are asymptotically independent of X. Using (5) and (11) enables the current to be entirely expressed by surface-projected objects

$$\left(X,\boldsymbol{K}_\parallel|G_2^+\Delta Q G_1^+ Q\Delta^+ G_2^-|X,\boldsymbol{K}_\parallel\right)=\tfrac{1}{p_x^z}\left(\boldsymbol{K}_\parallel|\mathcal{T}_2^+\mathcal{G}_{c2}^{+\,-1}\left[\mathcal{I}+\mathcal{M}\mathcal{G}_{c1}^{+\,-1}\left(\mathcal{G}_1^+-\mathcal{G}_{c1}^+\right)\mathcal{G}_{c1}^{+\,-1}\mathcal{N}\right]\mathcal{G}_{c2}^{-\,-1}\mathcal{T}_2^-|\boldsymbol{K}_\parallel\right), \tag{14}$$

where

$$\mathcal{I}\left(\boldsymbol{K}_\parallel+\boldsymbol{g}_\parallel,\boldsymbol{K}_\parallel+\boldsymbol{g}'_\parallel\right)=\left(0,\boldsymbol{K}_\parallel+\boldsymbol{g}_\parallel|G_{c2}^+\Delta Q G_{c1}^+ Q\Delta^+ G_{c2}^-|0,\boldsymbol{K}_\parallel+\boldsymbol{g}'_\parallel\right), \tag{15}$$

$$\mathcal{M}\left(\boldsymbol{K}_\parallel+\boldsymbol{g}_\parallel,\boldsymbol{K}_\parallel+\boldsymbol{g}'_\parallel\right)=\left(0,\boldsymbol{K}_\parallel+\boldsymbol{g}_\parallel|G_{c2}^+\Delta Q G_{c1}^+|0,\boldsymbol{K}_\parallel+\boldsymbol{g}'_\parallel\right), \tag{16}$$

$$\mathcal{N}\left(\boldsymbol{K}_\parallel+\boldsymbol{g}_\parallel,\boldsymbol{K}_\parallel+\boldsymbol{g}'_\parallel\right)=\left(0,\boldsymbol{K}_\parallel+\boldsymbol{g}_\parallel|G_{c1}^+ Q\Delta^+ G_{c2}^-|0,\boldsymbol{K}_\parallel+\boldsymbol{g}'_\parallel\right), \tag{17}$$

still have to be calculated. In the same way as for (7) and (10), but somewhat more lengthily, these integrals are obtained by contour integrations in the complex k_x-plane using the Fourier representation of Q, i.e.,

$$Q(x)=\mathrm{i}\lim_{\eta\to 0^+}\int\frac{\mathrm{d}k}{2\pi}\,\frac{\mathrm{e}^{\mathrm{i}kx}}{k+\mathrm{i}\eta}.$$

The integration path for calculating (7), (10) and (15)–(17) excludes all poles outside a strip of width of a Brillouin zone. Hence,

$$\begin{aligned}\mathcal{I}\left(\boldsymbol{K}_\parallel+\boldsymbol{g}_\parallel,\boldsymbol{K}_\parallel+\boldsymbol{g}'_\parallel\right)=&-\mathrm{i}\sum_{\alpha\beta}\sum_{g,g'}\sum_{g_r\cdots g_n}\sum_{k_+(2+)}\sum_{k''_-(2-)}\operatorname*{Res}_{k_+(2+)}\left(\boldsymbol{K}+\boldsymbol{g}|G_{c2}^+|\boldsymbol{K}+\boldsymbol{g}_r\right)\\&\times\Delta_\alpha\left(\boldsymbol{K}_+(2+)+\boldsymbol{g}_r\right)\Delta_\beta^+\left(\boldsymbol{K}''_-(2-)+\boldsymbol{g}_n\right)\delta\left(\boldsymbol{g}_{r\parallel},\boldsymbol{g}_{l\parallel}\right)\delta\left(\boldsymbol{g}_{m\parallel},\boldsymbol{g}_{n\parallel}\right)\\&\times\operatorname*{Res}_{k''_-(2-)}\left(\boldsymbol{K}''+\boldsymbol{g}_n|G_{c2}^-|\boldsymbol{K}''+\boldsymbol{g}'\right)\frac{1}{k_+(2+)-k''_-(2-)+g_r+g_m-g_n-g_l-\kappa_\alpha+\kappa_\beta^*}\\&\times\Bigg(\sum_{k'_+(1+)}\frac{1}{k'_+(1+)-k''_-(2-)+g_m-g_n+\kappa_\beta^*}\operatorname*{Res}_{k'_+(1+)}\left(\boldsymbol{K}'+\boldsymbol{g}_1|G_{c1}^+|\boldsymbol{K}'+\boldsymbol{g}_m\right)\\&+\sum_{k'_-(1+)}\frac{1}{k'_-(1+)-k_+(2+)+g_l-g_r+\kappa_\alpha}\operatorname*{Res}_{k'_-(1+)}\left(\boldsymbol{K}'+\boldsymbol{g}_l|G_{c1}^+|\boldsymbol{K}'+\boldsymbol{g}_m\right)\Bigg),\end{aligned} \tag{18}$$

$$\begin{aligned}&\mathcal{M}\left(\boldsymbol{K}_\parallel+\boldsymbol{g}_\parallel,\boldsymbol{K}_\parallel+\boldsymbol{g}'_\parallel\right)\\&=\mathrm{i}\sum_{\alpha}\sum_{g,g'}\sum_{g_i,g_j}\sum_{k_+(2+)}\sum_{k'_-(1+)}\operatorname*{Res}_{k_+(2+)}\left(\boldsymbol{K}+\boldsymbol{g}|G_{c2}^+|\boldsymbol{K}+\boldsymbol{g}_i\right)\Delta_\alpha\left(\boldsymbol{K}_+(2+)+\boldsymbol{g}_i\right)\\&\quad\times\delta\left(\boldsymbol{g}_{i\parallel},\boldsymbol{g}_{j\parallel}\right)\frac{1}{k_+(2+)-k'_-(1+)+g_i-g_j-\kappa_\alpha}\operatorname*{Res}_{k'_-(1+)}\left(\boldsymbol{K}'+\boldsymbol{g}_j|G_{c1}^+|\boldsymbol{K}'+\boldsymbol{g}'\right),\end{aligned} \tag{19}$$

$$\begin{aligned}&\mathcal{N}\left(\boldsymbol{K}_\parallel+\boldsymbol{g}_\parallel,\boldsymbol{K}_\parallel+\boldsymbol{g}'_\parallel\right)\\&=\mathrm{i}\sum_{\alpha}\sum_{g,g'}\sum_{g_i,g_j}\sum_{k_+(1+)}\sum_{k'_-(2-)}\operatorname*{Res}_{k_+(1+)}\left(\boldsymbol{K}+\boldsymbol{g}|G_{c1}^+|\boldsymbol{K}+\boldsymbol{g}_i\right)\Delta_\alpha^+\left(\boldsymbol{K}_-(2-)+\boldsymbol{g}_j\right)\\&\quad\times\delta\left(\boldsymbol{g}_{i\parallel},\boldsymbol{g}_{j\parallel}\right)\frac{1}{k_+(1+)-k'_-(2-)+g_i-g_j+\kappa_\alpha^*}\operatorname*{Res}_{k'_-(2-)}\left(\boldsymbol{K}'+\boldsymbol{g}_j|G_{c2}^-|\boldsymbol{K}'+\boldsymbol{g}'\right),\end{aligned} \tag{20}$$

where $\boldsymbol{K}_{\parallel}=\boldsymbol{K}''_{\parallel}\cong\boldsymbol{K}'_{\parallel}$ ($\kappa_{\parallel}$ is neglected). $k_+(E+)$ are the eigenvalues of the forward-propagating waves ($v_{2+}>0$, $\mathrm{Im}\,k_+>0$) and $k_-(E+)$ are the backward-propagating ones ($v_{2+}<0$, $\mathrm{Im}\,k_-<0$), respectively, where $E+$ denotes the corresponding retarded Green's function. Note that for the advanced functions (e.g. $2-$), forward-propagating waves ($v_{2-}>0$) correspond to k_-, i.e., $\mathrm{Im}(k_-(2-))<0$. The matrix element is simply given by

$$\Delta_\alpha\left(\boldsymbol{K}_+(2+)+\boldsymbol{g}_r\right)=A_{x\alpha}\left(k_+(2+)+g_r-\tfrac{1}{2}\kappa_\alpha\right)+\boldsymbol{A}_{\parallel\alpha}\cdot\left(\boldsymbol{K}_{\parallel}+\boldsymbol{g}_{\parallel}-\tfrac{1}{2}\kappa_{\parallel}\right),$$
$$\Delta^+_\alpha\left(\boldsymbol{K}''_2(2-)+\boldsymbol{g}_n\right)=A^*_{x\alpha}\left(k''_-(2-)+g_n-\tfrac{1}{2}\kappa^*_\alpha\right)+\boldsymbol{A}_{\parallel\alpha}\cdot\left(\boldsymbol{K}''_{\parallel}+\boldsymbol{g}_{r\parallel}-\tfrac{1}{2}\kappa_{\parallel}\right). \tag{21}$$

The residuum of the Green's function at fixed $\boldsymbol{K}_{\parallel}$ and E is connected with the eigenvectors of real bands as follows

$$\operatorname*{Res}_{k_\pm}\left(\boldsymbol{K}+\boldsymbol{g}|G^+_c|\boldsymbol{K}+\boldsymbol{g}'\right)=\mp\frac{a^*_g a_{g'}}{|v|}, \tag{22}$$

where a_g are the Fourier coefficients of the Bloch wave. Eq. (22) results from the spectral representation of G. The different contributions to the current are easy to extract from (14). Bulk contributions correspond to the poles of $\mathscr{J}$ whereas surface-state contributions belong to the poles of $\mathscr{G}_1$. Nevertheless, the general formula should preferentially be used for the calculations, whereas for interpretations (14) should be decomposed into the pole contributions.

2.2. Emission from bulk states

The terms with $g=g'$ and $g_r=g_l=g_m=g_n$ yield the largest contribution to the pole of $\mathscr{J}$. With $E(k,\boldsymbol{k}_{\parallel})=E(k,-\boldsymbol{k}_{\parallel})$ and $E(\boldsymbol{k})=E^*(\boldsymbol{k}^*)$, the prefactor before the parentheses, i.e.,

$$\left(k_+(2+)-k_-(2-)-2\mathrm{i}\,\mathrm{Im}\,\kappa_\alpha\right)^{-1}=\tfrac{1}{\mathrm{i}}\left(l^{-1}+\xi_\alpha^{-1}\right)^{-1}, \tag{23}$$

is essentially determined by the electron mean free path $l=v_2/\gamma_2$ for transversal fields ($\xi_T\gg l$), whereas the contribution from longitudinal fields may be reduced owing to a strong attenuation. The terms in the parentheses of (18) represent the "quasi-$k_\perp$-conservation" for bulk peak transitions. Which of these terms is predominant depends on the sign of v_1. The first term corresponds to a direct transition from an initial state band with a forward-propagating wave, whereas the second belongs to a backward-propagating one. Particularly the second term yields the essential bulk band transition near a local gap, where v_1 and v_2 have opposite signs. Linear expansion of the initial and final state bands, presuming transitions far from the critical points and using (22), for the longitudinal and transversal contributions to the current yields

$$\mathscr{J}_\alpha=\mathscr{F}_\alpha\frac{1}{\gamma_2}\,\frac{1}{\epsilon+\mathrm{i}\tilde{\gamma}_{\mathrm{b}\alpha}/2}, \tag{24}$$

$$\mathscr{F}_\alpha=\frac{1}{|v_1|+v_2}\sum_g\sum_{g_r}|a_g(2)|^2|a_{g_r}(2)|^2|a_{g_r}(1)|^2|\Delta_\alpha\left(\boldsymbol{K}_+(2+)+\boldsymbol{g}_r\right)|^2, \tag{25}$$

$$\tilde{\gamma}_{\mathrm{b}\alpha}=\left(\frac{\gamma_1}{|v_1|}+\frac{\gamma_2}{|v_2|}+\xi_\alpha^{-1}\right)\left|\frac{1}{|v_1|}\left(1-\frac{v_{1\parallel}\sin^2(\theta)}{k_{\parallel}}\right)-\frac{1}{|v_2|}\left(1-\frac{v_{2\parallel}\sin^2(\theta)}{k_{\parallel}}\right)\right|^{-1}, \tag{26}$$

where ϵ is the energy with respect to the peak maximum, and the interference terms between the different field contributions are neglected. $\mathscr{F}_\alpha$ weakly depends on the energy. The FWHM of the peak originating from bulk transitions agrees with (1) for $\xi_T\gg l$, which can also be illustrated by geometric considerations in the local band structure scheme [4,8]. However, in general, the broadening contribution from longitudinal fields cannot be neglected. The intensity of bulk peaks is essentially determined by γ_2, which is also plausible. Note that the same result (1) is obtained from (2) with neglected projection Q.

2.3. Emission from surface states

The surface state peak in photoemission spectra is determined by the pole of $\hat{\mathscr{G}}_1$. Consequently, the FWHM of that peak is independent of Σ_2, i.e., the optical potential for electrons:

$$\hat{\mathscr{G}}_1 = \hat{\mathscr{A}}/\left(E_1 - E_s(\boldsymbol{k}_\parallel) - \Sigma_1\right), \tag{27}$$

$$\hat{\mathscr{A}} = \hat{\mathscr{B}}_1\left(\frac{\mathrm{d}}{\mathrm{d}E}\det\left(\mu_\mathrm{b}\hat{\mathscr{L}}_\mathrm{b} - \mu_\mathrm{c}\hat{\mathscr{L}}_\mathrm{c}\right)\Big|_{E_s(\boldsymbol{k}_\parallel)}\right)^{-1}. \tag{28}$$

$\hat{\mathscr{B}}_1$ is the algebraic complement to $\hat{\mathscr{G}}_1^{-1}$. Contrary to bulk state transitions, which are characterized by poles with respect to $k_\perp$, here the pole is given solely by the initial state energy. Expansion with respect to the peak maximum yields $\tilde{\gamma}_s$ formally obtainable from (1) with $v_1 = 0$. However, the FWHM strongly depends on surface imperfections [5–7]. For example, assuming a local surface impurity potential in the simplest way yields

$$V(\boldsymbol{r}) = \delta(x)\sum_{\rho_i} V(\rho - \rho_i). \tag{29}$$

Then averaging Eq. (5) is restricted to the surface projection

$$\left\langle\hat{\mathscr{G}}(\boldsymbol{k}_\parallel E)\right\rangle = \left(\hat{\mathscr{G}}_0^{-1}(\boldsymbol{k}_\parallel E) - \hat{\Sigma}_i(\boldsymbol{k}_\parallel E)\right)^{-1}, \tag{30}$$

where the notation $\hat{\mathscr{G}}_0$ here concerns the impurity-free surface and $\hat{\Sigma}_i$ includes surface scattering in a certain approximation. In general, there is no simple separation in band and self-energy parts in the form of (27) since the surface projection $\hat{\mathscr{G}}_0$ is not a true propagator. If neglecting surface corrugation, the contribution of impurities to the FWHM γ_i is given by

$$\gamma_i = -2\ \mathrm{Im}\ \Sigma_i(\boldsymbol{k}_\parallel E)\left(\frac{\mathrm{d}}{\mathrm{d}E}\left(\mu_\mathrm{b}\mathscr{L}_\mathrm{b} - \mu_\mathrm{c}\mathscr{L}_\mathrm{c}\right)\Big|_{E_s(\boldsymbol{k}_\parallel)}\right)^{-1}, \tag{31}$$

which in contrast to the hole contribution shows a scaling of the corresponding self-energy by the surface state intensity factor [15]. $\boldsymbol{k}_{\parallel\mathrm{s}}$ corresponds to the surface state, i.e., $E_1 = E_\mathrm{s}(\boldsymbol{k}_{\parallel\mathrm{s}})$. Besides the broadening due to limited angular resolution, the intrinsic effect of the peak width depending on band dispersion is sometimes called non-lifetime effect [5]. Kevan assumes a constant impurity cross section of potassium trace impurities on Cu(111), concluding a linear increase of the FWHM via quadratic surface band dispersion [7]. This dispersive effect can be verified by calculating $\Sigma_i(\boldsymbol{k}_\parallel, E)$ in Born's approximation using a potential $V(\rho)$ in Eq. (29) with a certain lateral extent [19].

The effective mass of the surface state band is obtained by using the expansion of the pole up to the order of $k_\parallel^2$:

$$E_\mathrm{s} = E_0 + \tilde{\mu}\boldsymbol{k}_\parallel^2, \tag{32}$$

$$\tilde{\mu} = \frac{1}{2}\frac{\partial^2}{\partial \boldsymbol{k}_\parallel^2}\det\left(\mu_\mathrm{b}\hat{\mathscr{L}}_\mathrm{b} - \mu_\mathrm{c}\hat{\mathscr{L}}_\mathrm{c}\right)\left(\frac{\mathrm{d}}{\mathrm{d}E}\det\left(\mu_\mathrm{b}\hat{\mathscr{L}}_\mathrm{b} - \mu_\mathrm{c}\hat{\mathscr{L}}_\mathrm{c}\right)\right)^{-1}\Bigg|_{E_0}. \tag{33}$$

For isotropic mass and neglected lateral corrugation, this expression is simplified to

$$\tilde{\mu}_0 = \frac{\mu_\mathrm{b}^2\dfrac{\partial\mathscr{L}_\mathrm{b}}{\partial E} - \mu_\mathrm{c}^2\dfrac{\partial\mathscr{L}_\mathrm{c}}{\partial E}}{\mu_\mathrm{b}\dfrac{\partial\mathscr{L}_\mathrm{b}}{\partial E} - \mu_\mathrm{c}\dfrac{\partial\mathscr{L}_\mathrm{c}}{\partial E}}. \tag{34}$$

For at least the homogeneous effective mass junction, i.e., for $\mu_b = \mu_c = 1/2$, the result (34) is in contradiction to experimental findings which refute the assumptions. There are considerable deviations of the effective mass from the free electron value also for image states. Giesen et al. explain these deviations by the shrinking gap [20]. Thus lateral corrugations have to be taken into account in calculations if the effective mass of the surface state is considered.

The intensity of the surface state is essentially determined by the prefactors of the pole-producing $\mathscr{G}$, i.e., $\mathscr{N}$ and $\mathscr{M}$. It is well known that the intensity shows maxima at certain photon energies [11–14]. In fact, these resonances can be interpreted as being a consequence of "quasi-$k_\perp$-conservation" applied to surface states. This is revealed by comparing the poles of $\mathscr{S}$, $\mathscr{M}$ and $\mathscr{N}$. However, note that for surface states peak widths and intensities belong to different poles. The phenomenon of intensity resonances is explicitly demonstrated by (19) and (20) with $E_1 = E_s$. The functions have maxima at final state energies with extended-zone-scheme wave vectors $K_2(E_s + \omega_n)$, fulfilling $\mathrm{Re}(K_2(E_s + \omega_n) - k_s) = ng$, where $k_s = k(E_s)$ is the surface state wave vector. There are resonances at ω_n for which K_2 is an odd integer of k_0 for a sp-band gap at the Brillouin zone boundary ($\mathrm{Re}(k_1) = k_0$). The distance between the resonances is $\omega_{n+1} - \omega_n = 4nk_0^2$. Since the first intensity maximum is near the vacuum level (top of the gap) and k_0^2 is in the order of ten electron volts, the second has a typical value of 40–60 eV.

3. Example: Cu (111)

The noble metal surfaces have extensively been investigated both theoretically and experimentally. For our aims, Cu(111) is especially suitable to illustrate lifetime effects in sp-bands since well-developed sp-band peaks are observed for very low photon energies ($\omega < 12$ eV) being sufficiently separated from the d-bands [1,31]. The nearly-free-electron two-band model shows a simple complex band structure to reveal surface states and to provide initial and final states for photoelectronic excitation. Normal emission at low energies allows one to restrict oneself to $\boldsymbol{K}_\parallel = 0$ and $\boldsymbol{g}_\parallel = 0$. For the real potential, the model of Lenac et al. [21] is used, which is shown in Fig. 1. It has been applied by many authors in a more or less special version in order to calculate image potential states or quantum well states. The bound states can be calculated by using either the phase

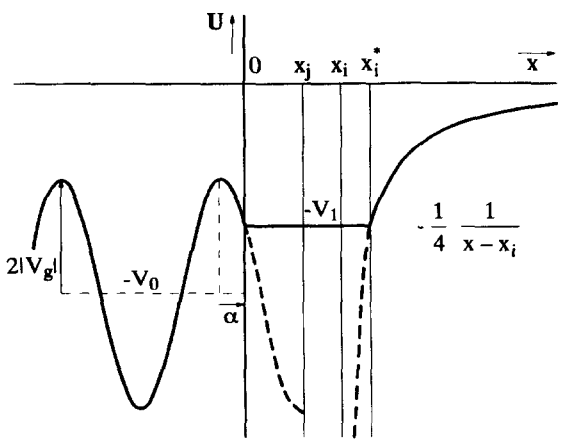

Fig. 1. The model potential. The bulk parameters V_0 and V_g correspond to the L-gap of Cu(111). At x = 0 there is the matching plane, whereas x_j and x_i denote the jellium edge and the image plane, respectively. x_i^* and α depend on the bottom of the surface potential V_1.

Table 1
Band parameters of Cu

$\lvert V_g\rvert$	$L_{2'}$	Γ_1	Work function (111)
2.48 eV	−0.9 eV	−8.73 eV	4.86 eV

accumulation method or det $\mathscr{G}^{-1} = 0$ with $\mathscr{G}$ determined by Eq. (9). The crystal potential in the one-dimensional nearly-free-electron form

$$U(x) = -V_0 + 2|V_g|\cos(gx + \alpha) \tag{35}$$

is terminated at the matching point $x = 0$, which is fixed between the outermost atomic layer (position of the maximum of $U(x)$) and the jellium edge x_j (position of minimum of $U(x)$). V_0 is determined by the energy at the band bottom Γ_1 and the work function, and the position of the gap of size $2|V_g|$ is given by the lower band edge $L_{2'}$. On the other hand, the image potential with the image plane position x_i is truncated in a way that the potential $-V_1$ continuously matches the crystal potential at $x = 0$. x_i and x_j do not coincide in general but x_i is slightly outside the jellium. α and x_i are the true free parameters of the model, whereas V_1 is fixed by α and the value of the work function. The surface bound states sensitively depend on these parameters. Since we are considering solely crystal-induced surface states in this paper, we restrict ourselves to a single free parameter α, which was shown [21] to be crucial, i.e., we set $x_i = x_j$. Note, however, that for α fixed the surface state energy is reduced by enlarging the trapping region. For that reason, on the other hand, some authors fix α and choose x_i to be the free parameter [22,23]. The binding energy of 0.4 eV of the Cu(111) surface state corresponds to $\alpha = 0.32$. The band parameters which are used in the calculations are summarized in Table 1.

The potential is completed by a homogeneous complex energy-dependent optical potential. In order to describe damping of the initial and final state, it suffices to use two pure imaginary functions σ_1 and σ_2. The wave vector with respect to $k_0 = g/2$ fulfils

$$\begin{aligned}
&\mu\kappa^2 = \epsilon + 2\mu k_0^2 - D(\epsilon),\\
&D(\epsilon) = \sqrt{\left(\epsilon + 2\mu k_0^2\right)^2 + |V_g|^2 - \epsilon^2},\\
&\epsilon = E - \mu k_0^2 - \sigma,
\end{aligned} \tag{36}$$

where κ should not be confounded with the wave vectors κ_α of the electromagnetic field. The reduced zone is chosen such that $-k_0 < \kappa < k_0$. The two complex solutions represent a pair of ingoing and outgoing Bloch waves. The branches of the roots should be chosen such that $\mathrm{Im}(k_+(E+)) > 0$ and $\mathrm{Im}(k_-(E+)) < 0$. Further solutions to the original eigenvalue equation do not contribute to the integrals since they are outside the reduced zone. The residues of the Green's functions are

$$\operatorname*{Res}_{\kappa_\pm} \boldsymbol{G}_c = \frac{1}{2\mu^2\kappa_\pm D}\begin{pmatrix} \mu\kappa_\pm^2 - 2\mu k_0\kappa_\pm - \epsilon & -|V_g|e^{i\alpha} \\ -|V_g|e^{-i\alpha} & \mu\kappa_\pm^2 + 2\mu k_0\kappa_\pm - \epsilon \end{pmatrix}, \tag{37}$$

which according to $\epsilon_\pm = \epsilon \pm i\gamma/2$ and taking into account $\kappa_+(\epsilon_+) = \kappa_-^*(\epsilon_-) = -\kappa_-(\epsilon_+)$ correspond to $\boldsymbol{G}^+$ and $\boldsymbol{G}^-$. All crystal-dependent functions $\mathscr{G}_c$, ${}'\mathscr{G}_c^+$, $\mathscr{J}$, $\mathscr{M}$ and $\mathscr{N}$ are fully determined by (36) and (37).

$\boldsymbol{G}_b$ and its surface projected objects in (9) are determined by numerical integration using a real surface potential. According to (8) and taking into account $\psi_2 = \psi_1^*$, ψ_1 has to be calculated. Inspecting (13) suggests the amplitude to be split off the amplitude yielding $\psi_1 = \eta(x)e^{ipx}$. The amplitude $\eta(x)$ is then determined by a transformed equation obtained by inserting this form into the Schrödinger equation. The integration for the image potential is performed starting at point x^* far away from the surface where $\eta(x^*) = 1$, $d\eta(x^*)/dx = 0$. In a similar manner, G_b is determined for $E < E_v$.

The wave vectors of longitudinal and transverse fields in (21) are determined by the corresponding dielectric functions. Then the amplitudes are calculated by using Fresnel equations for metal optics which include plasma waves. This has been discussed in detail in literature [24–26] so that the derivation of these equations will not be pointed out again. By the definition of the matching plane, the internal field is used for calculating both bulk state and surface state. The calculation of the surface photoemission arising from the barrier would also require the careful determination of the field in the barrier region. As mentioned above, this is neglected in the present paper. The (transverse) dielectric function $\epsilon(\omega)$ is given by

$$\epsilon(\omega) = 1 - \frac{\omega_p^2}{\omega^2} + 4\pi\chi(\omega), \tag{38}$$

where ω_p is the plasma frequency. For the interband contributions

$$4\pi\chi(\omega) = i\frac{\chi_0}{\sqrt{\omega^2 - 4|V_g|^2}} \tag{39}$$

is used. This expression contains the essential square root singularity, which can be derived in the two-band model [27], but the analytical structure is much simpler than the exact one. The exact result [28], however, permits one to estimate the value of χ_0. The expression of

$$\chi_0 = \frac{8}{3}\frac{|V_g|^2}{G}\frac{(\tilde{\omega}_2 - \omega_p)(\omega_p - \tilde{\omega}_1)}{\omega_p^3} \tag{40}$$

yields $\chi_0 = 0.249$, if the band parameters $\tilde{\omega}_1 = 0.114$, $\tilde{\omega}_2 = 2.43$, and the plasma frequency $\omega_p = 0.261$ (in atomic units) are used. The longitudinal wave vector is determined by

$$\epsilon_L = 1 + \frac{4\pi i}{\omega}\sigma_L = 0, \tag{41}$$

where the hydrodynamical model [26] yields

$$\sigma_L = \frac{i\omega}{4\pi}\frac{1}{(1-\epsilon)^{-1} - \frac{\beta}{\omega_p^2}\kappa_\parallel^2}. \tag{42}$$

Formula (42) is also assumed to be valid if the interband contribution is taken into account. The second term in the denominator arising from the Fermi gas pressure ($\beta = \frac{3}{5}v_F^2$, v_F is the Fermi velocity) causes a strong nonlocality of the longitudinal field. Using Maxwell's equations and (41) and (42) yields

$$\kappa_T = \sqrt{\frac{\omega^2}{c^2}\epsilon(\omega) - \kappa_\parallel^2}, \tag{43}$$

$$\kappa_L = \sqrt{\frac{\omega_p^2}{\beta}\frac{\epsilon(\omega)}{(1-\epsilon(\omega))} - \kappa_\parallel^2}, \tag{44}$$

which verifies that κ_L/κ_T is of the order of $c/v_F \approx 100$.

At very low energies ($E_2 - E_F < 10$ eV) the electron inverse lifetime strongly depends on energy. For a free electron gas the dependence [29] is given by

$$\gamma_2 = \lambda\left(\sqrt{\frac{E}{E_F}} - 1\right)^2, \tag{45}$$

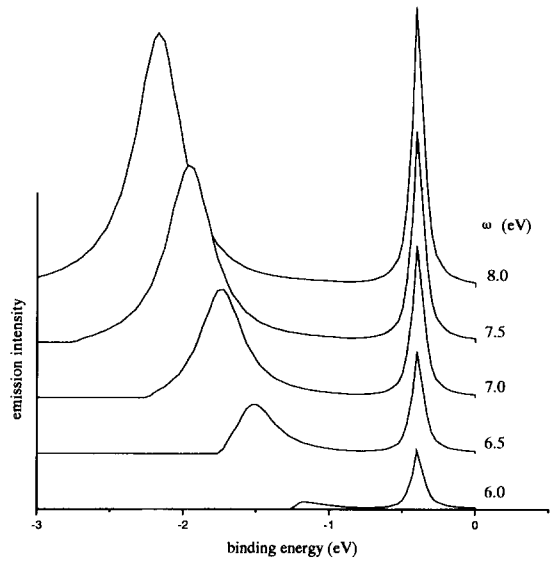

Fig. 2. Calculated normal-emission spectra for p-polarized light with the angle of incidence $\varphi = 30°$ and photon energies of $6 \leqslant \omega \leqslant 8$ eV with $\lambda = 5.0$ eV.

which was verified to be valid up to approximately $E/E_F < 2.5$ [30]. Here the energy refers to the Γ-point. Parameter λ can be determined from photoemission by comparison with calculations. From theory [29],

$$\lambda_{QF} = \left(\frac{\pi}{4br_s}\right)^{3/2} \times 13.6 \text{ eV} \tag{46}$$

is obtained with $b = 0.521$ and r_s being the electron density parameter. For Cu, one gets $\lambda_{QF} = 5.7$ eV. The electron inverse lifetime obtained from fitting the FWHM of d-band peaks [1] with Eq. (45) approximately yields $\lambda_{KHE} = 4.9$ eV, where the enlarged value of $E_F = 8.7$ eV is used owing to the hybridization with d-bands. The discrepancy between these λ-values is explained by the large Fermi-surface anisotropy of Cu, which is neglected in the derivation of Eq. (46). In contrast to γ_2, the intensities are nearly independent of γ_1 as it can be deduced from (24) and from calculations. Therefore here, unlike to the peak width, it is not necessary to take into account the energy dependence of γ_1. Moreover, Knapp et al. [1] observed a weak energy dependence of the inverse hole lifetime for binding energies below 2 eV. As it is insignificant for intensities, we use their estimate of 0.2 eV in spite of even smaller values cited in the literature [3]. A series of spectra calculated for sp-bands is shown in Fig. 2 using $\lambda = 5.0$ eV and the angle of incidence $\varphi = 30°$ [31]. Fig. 3 shows the ratio of bulk-to-surface state peak intensities for various λ values. The intensities are determined by Lorentz-fits, which in the calculations correspond to the residua of Eqs. (14), (24) and (27), by using (26). The experimental bulk-to-surface state ratios are obtained from the spectra published by Knapp et al. [1], and by Gartland and Slagsvold [31]. The errors are due to the estimation from their published figures. Especially the surface state intensity taken from Knapp's spectra implies some uncertainty, and the bulk state intensities for very low energies also have errors because of the low intensities and the small separation from the surface state. In the range of $8 < \omega < 10$ eV no values are available owing to the crossing with the d band. Estimations from spectra for energies larger than 10 eV approximately correspond to λ_{KHE}, or slightly below, which verifies that the intensity ratio is mainly determined by electron lifetimes. The experimental curve shows a more pronounced maximum at about 11 eV, whereas the respective calculation yields a maximum at about 9 eV. At low energies the intensity ratio calculated with $\lambda = 6$ eV agrees well with the result of Gartland and Slagsvold [31], but for

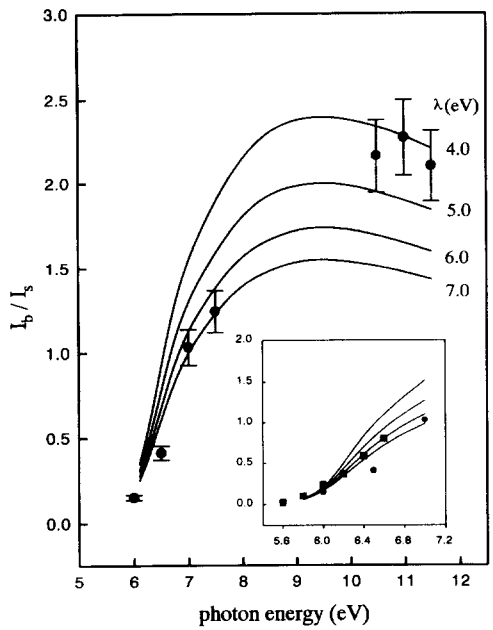

Fig. 3. The bulk-to-surface state intensity ratio calculated for various λ-values and $\varphi = 30°$. The experimental values are obtained from Knapp et al. (● from Ref. [1]) and from Gartland and Slagsvold (■ from Ref. [31]). The error is due to the estimating procedure of the values from the spectra. The inset magnifies the threshold region.

higher energies the value of λ which yields coincidence with experiments is smaller. The main reasons for the deviation from λ_{QF} are the rough approximations of the bands by NFE bands and of the dielectric function. Furthermore, the nearer the energy approaches the band gap the larger is the effect of anisotropy. The surface state intensity weakly depends on λ since the electron mean free path is much larger than the surface state decaying length ζ. Thus the effective information depth for the surface state is saturated to ζ for which the NFE calculation yields the value of 8.7 Å. The actual value is approximately half the NFE value [13]. This discrepancy corresponds to an incorrect effective mass at the band bottom obtained from NFE calculations [13]. The surface state intensity as a function of photon energy only decreases at higher photon energies. For low energies the surface barrier (work function and electron transmission) should be considered. The inset of Fig. 3 shows the intensity near the threshold. Calculations from (12) reveal, however, the transmission amplitude $|\mathcal{T}_2^+|$ to differ from the function for the step potential by less than 10% for energies larger than 1 eV above the vacuum threshold. In other words, the transmission is not important for intensity ratios. The correct barrier potential is required to obtain the surface state with binding energies below the Fermi energy.

4. Conclusions

The peak intensities arising from surface states and bulk states are calculated in dependence on inverse lifetimes of holes and electrons, which are given by the imaginary parts of the corresponding optical potentials $-\gamma_1/2$ and $-\gamma_2/2$, respectively. The intensities are almost independent of γ_1, whereas the bulk peak strongly increases with decreasing γ_2. Thus the ratio of bulk-to-surface state intensities directly depends on electron lifetime since it is also unaffected by instrumental broadening. For Cu(111) the intensity analysis yields a reasonable agreement with lifetimes estimated from FWHM. At very low photon energies ($\omega < 8$ eV) the intensity analysis yields values larger for the inverse electron lifetime than estimated for homogeneous electron

gas. In contrast to γ_2, γ_1 can be determined solely by measuring the peak widths. Especially the peaks of surface states depend solely on γ_1, which includes the inverse hole lifetime as well as contributions by surface imperfections. The inverse hole lifetime contains a dispersive contribution if defects are laterally extended.

The calculation of the photoelectric current on the basis of Eq. (14) can be extended to quantum wells and layered systems where other methods often are not suitable. However, more realistic models are required especially to obtain the correct bands near the local gap as well as the optical matrix elements. Therefore, expressions (15) to (17) have to be calculated on a basis which is completed by atomic-like functions. In spite of being tested only for a very simple model the method of calculating photoelectron spectra on the basis of Green's function matching seems to work very efficiently.

Acknowledgements

The critical reading of the paper by W. Kuch is gratefully acknowledged.

References

[1] J.A. Knapp, F.J. Himpsel and D.E. Eastman, Phys. Rev. B 19 (1979) 5952.
[2] S.D. Kevan and D.A. Shirley, Phys. Rev. B 22 (1980) 542.
[3] S.D. Kevan, Phys. Rev. Lett. 50 (1983) 526.
[4] J.K. Grepstad, B.J. Slagsvold and I. Bartoš, J. Phys. F 12 (1982) 679.
[5] J. Tersoff and S.D. Kevan, Phys. Rev. B 28 (1983) 4267.
[6] B.J. Slagsvold, J.K. Grepstad and P.O. Gartland, Phys. Scr. T 4 (1983) 65.
[7] S.D. Kevan, Surf. Sci. 178 (1986) 229.
[8] N.V. Smith, P. Thiry and Y. Petroff, Phys. Rev. B 47 (1993) 15476.
[9] J.B. Pendry, Surf. Sci. 57 (1976) 679.
[10] I. Bartoš and J. Koukal, Surf. Sci. 138 (1984) L151.
[11] S.G. Louie, P. Thiry, R. Pinchaux, Y. Petroff, D. Chandresris and J. Lecante, Phys. Rev. Lett. 44 (1980) 549.
[12] T.C. Hsieh, P. John, T. Miller and T.-C. Chiang, Phys. Rev. B 35 (1987) 3728.
[13] S.D. Kevan and R.H. Gaylord, Phys. Rev. B 36 (1987) 5809.
[14] S.D. Kevan, N.G. Stoffel and N.V. Smith, Phys. Rev. B 31 (1985) 3348.
[15] A. Beckmann, Phys. Status Solidi (b) 138 (1986) 295.
[16] F. Garcia-Moliner, Ann. Phys. (Paris) 2 (1977) 179.
[17] F. Garcia-Moliner, F. Flores, Introduction to the Theory of Solid Surfaces (Cambridge University Press, Cambridge, 1979).
[18] G. Paasch, Phys. Status Solidi (b) 87 (1978) 191.
[19] A. Beckmann, unpublished.
[20] K. Giesen, F. Hage, F.J. Himpsel, H.J. Riess, W. Steinmann and N.V. Smith, Phys. Rev. B 35 (1987) 975.
[21] Z. Lenac, M. Šunić, H. Conrad and M.E. Kordesch, Phys. Rev. B 36 (1987) 9500.
[22] N.V. Smith, Phys. Rev. B 32 (1985) 3549.
[23] M. Ortuño and P.M. Echenique, Phys. Rev. B 34 (1986) 5199.
[24] F. Sauter, Z. Phys. 203 (1967) 488.
[25] A.R. Melnyk and M.J. Harrison, Phys. Rev. B 2 (1970) 835.
[26] K. Kempa and F. Forstmann, Surf. Sci. 129 (1983) 516.
[27] G.D. Mahan, Phys. Rev. B 2 (1970) 4334.
[28] K. Sturm and L.E. Oliveira, Phys. Rev. B 30 (1984) 4351.
[29] J.J. Quinn and R.A. Ferrell, Phys. Rev 112 (1958) 812.
[30] B.J. Lundqvist, Phys. Status Solidi 32 (1969) 273.
[31] P.O. Gartland and B.J. Slagsvold, Phys. Rev. B 12 (1975) 4047.